
Predictive–Generative Drift Decomposition for Speech Enhancement and Separation

Julius Richter
MERL
Cambridge, MA, USA
richter@merl.com

Yoshiki Masuyama
MERL
Cambridge, MA, USA
masuyama@merl.com

Christoph Boeddeker
MERL
Cambridge, MA, USA
boeddeker@merl.com

Takahiro Edo
MERL
Cambridge, MA, USA
tedo@merl.com

Gordon Wichern
MERL
Cambridge, MA, USA
wichern@merl.com

Jonathan Le Roux
MERL
Cambridge, MA, USA
leroux@merl.com

Abstract

We propose a plug-and-play framework for speech enhancement and separation that augments predictive methods with a generative speech prior. Our approach, termed Stochastic Interpolant Prior for Speech (SIPS), builds on stochastic interpolants and leverages their flexibility to bridge predictive and generative modeling. Specifically, we decompose the interpolation dynamics into a task-specific drift and a stochastic denoising component, allowing a predictive estimate to be integrated directly into the generative sampling process. This results in a mathematically grounded framework for combining strong pretrained predictors with the expressive power of generative models. To this end, we train a score model using only clean speech, yielding a degradation-agnostic prior that can be reused across tasks. During inference, the predictor provides a deterministic drift that steers the sampling process toward a task-consistent estimate, while the score model preserves perceptual naturalness. Unlike prior hybrid approaches, which typically rely on architecture-specific conditioning and are tied to particular predictors or degradation settings, SIPS provides a unified framework that generalizes across predictors and additive degradation tasks. We demonstrate its effectiveness for both speech enhancement and speech separation using recent predictors such as SEMamba and FlexIO. The proposed method consistently improves perceptual quality, achieving gains up +1.0 NISQA for speech separation.

1 Introduction

Learning-based methods for speech enhancement and speech separation have achieved remarkable progress over the past decades [3]. Modern neural architectures trained in a supervised manner are capable of producing highly accurate reconstructions and have substantially advanced both instrumental (objective) metrics and subjective human ratings of speech quality [19]. Existing approaches can be broadly categorized into predictive and generative models.

Predictive models dominate the field [4, 7, 22, 36, 37]. These methods directly estimate the clean speech signal from degraded observations using regression-based objectives. With sufficient training data and architectural capacity, predictive models achieve excellent signal-level metrics and strong performance. However, because they are optimized for point estimates, they can produce perceptually unpleasant artifacts in challenging scenarios, such as extremely low signal-to-noise ratios (SNRs),

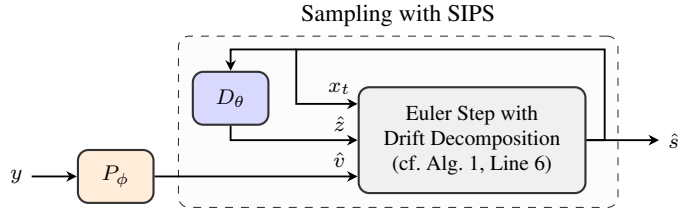


Figure 1: Overview of the proposed plug-and-play framework. A pretrained predictor P_ϕ defines a deterministic drift $\hat{v} = P_\phi(y) - y$ from the observation y , which steers the sampling dynamics at every step. Concurrently, the denoiser D_θ guides the trajectory toward regions of higher likelihood.

heavy reverberation, or domain mismatch. In such cases, the model may over-suppress, leak the interfering signal, or generate unnatural distortions that degrade perceptual quality [9].

Generative models offer a complementary perspective. Instead of learning a deterministic mapping, they aim to model the distribution of clean speech signals S by learning a prior distribution ρ_S over the data. Given a noisy observation Y , restoration is then formulated as an inference problem, where samples are drawn or approximated from the posterior distribution $p_{S|Y}$ under an assumed observation model [18]. In addition, many approaches adopt a conditional formulation, where the generative model is explicitly conditioned on the observation and is designed to approximate the posterior $p_{S|Y}$, as in conditional diffusion or score-based methods such as SGMSE [27, 39]. However, this expressive power comes at a cost: generative restoration methods are prone to hallucinations, inconsistencies with the observation, and reduced faithfulness to the underlying signal, especially when the conditioning signal is weak or ambiguous [6, 9].

These observations suggest a fundamental trade-off. Predictive models are typically faithful to the observed signal and excel on signal-level objective metrics such as SI-SDR [15] and PESQ [31], but can sound perceptually unnatural under difficult conditions. In contrast, generative models often produce more natural and perceptually pleasing outputs, which is reflected in strong performance on non-intrusive (reference-free) or system-level metrics such as DNSMOS [26]. Such inconsistencies can be quantified using downstream tasks, for example by evaluating automatic speech recognition (ASR) performance and measuring the resulting word error rate (WER). Ideally, a speech restoration system should combine the strengths of both paradigms, achieving high perceptual quality while remaining faithful to the underlying content. Bridging this gap remains an open challenge.

In this work, we propose Stochastic Interpolant Prior for Speech (SIPS), a plug-and-play framework that combines the strengths of both paradigms. Our approach augments existing predictive speech restoration systems with a generative clean-speech prior learned via score modeling [35]. The score model is trained using only clean speech, yielding a degradation-agnostic prior that does not depend on a specific corruption process. At inference time, the output of a pretrained predictive model P_ϕ defines a deterministic drift term \hat{v} that guides the sampling process toward a task-consistent estimate (see Fig. 1). In parallel, the learned score function or denoiser D_θ estimates the Gaussian noise and steers the trajectories toward regions of higher likelihood, thereby enforcing consistency with the distribution of natural speech and improving perceptual realism. This decomposition enables the predictor to maintain fidelity to the observation, while the generative prior mitigates artifacts and enhances naturalness.

We evaluate the proposed framework on speech enhancement and speech separation using recent high-performing predictors, including SEMamba [4] and FlexIO [24]. Across tasks and models, our method consistently improves non-intrusive perceptual quality scores, indicating enhanced naturalness, while incurring only minor decreases in reference-based distortion metrics. These results demonstrate that predictive and generative modeling need not be competing paradigms, but can be combined in a principled and complementary manner. Our implementation is publicly available¹.

¹<https://github.com/merlresearch/sips-speech>

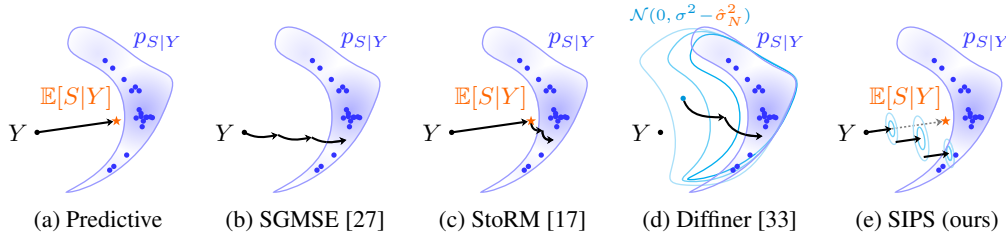


Figure 2: Overview of different modeling approaches for speech enhancement: (a) Predictive models learn a deterministic mapping that approximates the posterior mean $\mathbb{E}[S|Y]$; (b) SGMSE learns the posterior distribution $p_{S|Y}$ by conditioning on the noisy observation Y ; (c) StoRM uses the predictive mapping as an intermediate step for generative inference of posterior samples; (d) Diffiner follows DDRM and uses the predictor output as an estimate of the noise variance $\hat{\sigma}_N^2$ to sample from a modified prior, combining the clean speech estimate with the observation at each step; (e) SIPS samples trajectories by decomposing the dynamics into a predictor-induced drift and a generative component.

2 Related Work

A significant breakthrough in audio restoration tasks, including speech enhancement and separation, came with the introduction of diffusion models, which have demonstrated substantial improvements in perceptual quality and robustness [18]. Since then, multiple diffusion variants have been proposed for speech enhancement and separation, including approaches using flow matching [16, 34, 40] and Schrödinger bridges [12, 29].

A congruent line of research investigates hybrid approaches that combine the strengths of predictive and generative models. Figure 2 provides an overview of different modeling paradigms for speech enhancement, including predictive, generative, and hybrid approaches. StoRM [17] introduces a stochastic regeneration model in which a diffusion process is trained conditional on the output of a predictor network, with both the predictor and the score model instantiated using the NCSN++ [35] architecture. Diffiner [33] is a diffusion-based refinement framework trained solely on clean speech. Building on Denoising Diffusion Restoration Models (DDRM) [14], it combines pretrained speech enhancement models, including Wave-U-Net [36] and DCU-net [7], with a diffusion prior through posterior sampling.

However, these hybrid approaches remain limited in flexibility and efficiency. StoRM requires the generative model to be trained jointly with, or explicitly conditioned on, the output of a specific predictor, restricting its ability to generalize across predictive backbones in a plug-and-play manner. Diffiner, on the other hand, relies on heuristic parameter choices and computationally expensive diffusion posterior sampling [14], typically requiring hundreds of reverse steps at inference (see Appendix C.6). By contrast, our approach trains a degradation-agnostic prior solely on clean speech and embeds predictor guidance directly into the stochastic interpolant dynamics, enabling plug-and-play integration with different predictors using only a small set of interpretable hyperparameters and substantially fewer sampling steps. Furthermore, the original Diffiner formulation was primarily studied for speech enhancement using earlier-generation predictors, while speech separation requires additional task-specific modifications [11].

3 Method

Score-based generative models (SGMs) [35] and flow-based models [2, 20, 21] have emerged as two prominent frameworks for generative modeling. We adopt stochastic interpolants [2], which provide a unified formulation of these approaches by constructing stochastic paths between variables via simple interpolation. Within this framework, we propose to combine a predictor-induced drift with an unconditional score model by decomposing the overall drift term in the stochastic differential equation (SDE)-based sampling scheme in a mathematically principled manner. This yields a coherent integration of predictive and generative models without ad hoc weighting rules, while maintaining a flexible formulation.

Notations. In the following, uppercase letters (e.g., X) denote random variables, and lowercase letters (e.g., x) their realizations. All random variables are defined on a common probability space. For a random variable X , we write ρ_X for its distribution (or density when it exists). For clarity, we present the formulation in the one-dimensional setting, however, all results extend naturally to higher-dimensional representations such as spectrograms, where each time–frequency bin is treated independently. Note, however, that the neural networks used to estimate the drift components operate on the entire input spectrogram.

3.1 Interpolant design and noise schedule

Stochastic interpolants [2] define a continuous family of random variables that smoothly connect two distributions through controlled noise injection, enabling generative modeling using ordinary differential equations (ODEs) or SDEs for sampling. A more detailed background is provided in Appendix A.

We define a linear stochastic interpolant between clean speech S and corrupted speech Y as

$$X_t = tS + (1 - t)Y + \gamma(t)Z, \quad t \in [0, 1], \quad (1)$$

where $(S, Y) \sim p_{S, Y}$ are jointly sampled from paired clean and corrupted speech signals, $Z \sim \mathcal{N}(0, 1)$ denotes a standard Gaussian random variable independent of (S, Y) , and $\gamma(t)$ is a scalar noise schedule. We parameterize the noise schedule as

$$\gamma(t) = c \sin^2(\pi t), \quad (2)$$

whose derivative with respect to t is

$$\dot{\gamma}(t) = c\pi \sin(2\pi t), \quad (3)$$

with hyperparameter $c \geq 0$. We use $c = 0.5$, selected via a small-scale hyperparameter search (see Appendix C.3).

Since $\gamma(0) = \gamma(1) = 0$, the interpolant in (1) becomes deterministic at the boundaries. Denoting the distribution of X_t at time t by ρ_t , we obtain $\rho_0 = \rho_Y$ and $\rho_1 = \rho_S$. The additive term $\gamma(t)Z$ injects Gaussian noise along the path, broadening the intermediate distributions and enabling stochastic exploration during generation.

3.2 Inference via stochastic dynamics

We begin by defining two key conditional expectations associated with the stochastic interpolant in (1). The first is the conditional velocity

$$v(t, x) = \mathbb{E}[\partial_t(tS + (1 - t)Y) | X_t = x] \quad (4)$$

$$= \mathbb{E}[S - Y | X_t = x], \quad (5)$$

which captures the expected time derivative of the interpolation path given the current state. The second is

$$\eta_z(t, x) = \mathbb{E}[Z | X_t = x], \quad (6)$$

which represents the conditional expectation of the injected noise.

Following Albergo et al. [2], it can be shown that, for each $t \in [0, 1]$, the distribution of the interpolant defined in (1) coincides with that of a stochastic process $(X_t^F)_{t \in [0, 1]}$ evolving according to the forward SDE (see Appendix A.5 for a derivation)

$$dX_t^F = (v(t, X_t^F) + (\dot{\gamma}(t) - \kappa)\eta_z(t, X_t^F))dt + \sqrt{2\kappa\gamma(t)}dW_t, \quad (7)$$

where W_t is a standard Wiener process and $\kappa \geq 0$ is a noise scaling parameter. Notably, for $\kappa = 0$, the SDE reduces to an ODE.

Although the stochastic interpolant in (1) and the process X_t^F have identical time-marginal distributions, they generally do not induce the same probability measure on path space. Indeed, X_t^F is a Markov diffusion driven by a Wiener process, whereas the interpolant in (1) is obtained by fixing (S, Y, Z) and evaluating a deterministic interpolation path over time. Thus, the equivalence is marginal in time rather than an equality in law of the full trajectories.

Algorithm 1 Sampling with SIPS

Require: Observation y , predictor P_ϕ , denoiser D_θ , noise scaling parameter $\kappa \geq 0$, number of steps M , arbitrary time schedule $\{t_i\}_{i=0}^M$ with $t_0 = 0$, $t_M = 1$, and step sizes $\{\Delta t_i\}_{i=0}^{M-1}$ with $\Delta t_i = t_{i+1} - t_i$

Ensure: Clean speech estimate x_1

Initialization

1: $\hat{v} = P_\phi(y) - y$

2: $x_0 = y$

Euler–Maruyama Steps

3: **for** $i = 0$ to $M - 1$ **do**

4: $\hat{z} = D_\theta(t_i, x_{t_i})$

5: $z \sim \mathcal{N}(0, I)$

6: $x_{t_{i+1}} = x_{t_i} + (\hat{v} + (\dot{\gamma}(t_i) - \kappa)\hat{z})\Delta t_i + \sqrt{2\Delta t_i\kappa\gamma(t_i)}z$

7: **end for**

Post Processing (optional)

8: $x_1 \leftarrow P_\phi(x_1)$

9: **return** x_1

3.3 Predictive–generative drift decomposition for inference

During inference, only Y is observed, so instead of taking the conditional expectation given X_t in (5), we consider the conditional expectation given $Y = y$, namely $\mathbb{E}[S - Y|Y = y]$. This formulation resembles a predictive modeling problem, where the goal is to estimate the target S from the input Y . Motivated by this perspective, we approximate the velocity field as

$$\hat{v}(y) = P_\phi(y) - y, \tag{8}$$

where P_ϕ denotes a predictive model parameterized by ϕ .

Given a pretrained predictor P_ϕ , clean speech is obtained by numerically integrating the SDE in (7), starting from the initialization $X_0 = Y$. During integration, the intractable term $\eta_z(t, x_t)$ is replaced by a learned denoiser $D_\theta(t, x_t)$. We discretize the SDE using a time grid $\{t_i\}_{i=0}^M$ with $t_0 = 0$ and $t_M = 1$. In our experiments, we use a uniform grid with $M = 15$ steps. This yields Algorithm 1, which produces the clean speech estimate X_1 from the observation Y .

Although the predictor can optionally be applied again as a post-processing step for speech enhancement to mitigate residual estimation errors, we found that this provides no consistent improvement in performance and therefore do not use it in our main experiments. The effect of this post-processing step is discussed in Appendix C.5.

3.4 Denoiser training

We train an unconditional score model or denoiser independently of corrupted observations by injecting Gaussian noise into clean speech samples. Since the interpolant noise level $\gamma(t)$ vanishes at the boundaries, we introduce a small constant $a \geq 0$ to ensure a non-degenerate noise level for all $t \in [0, 1]$. This stabilizes training by requiring the model to estimate noise even near the endpoints. The resulting objective is

$$\min_{\theta} \mathbb{E} \left[\|D_\theta(t, S + (a + \gamma(t))Z) - Z\|^2 \right], \tag{9}$$

where $t \sim \text{Uniform}[0, 1]$, $S \sim \rho_S$, and $Z \sim \mathcal{N}(0, I)$ is a standard Gaussian random variable with identity covariance matrix I . Note that this training setup corresponds to so-called mirror interpolants [2]. See Appendix A.4 for more details. We use $a = 0.1$, selected via a small-scale hyperparameter search (see Appendix C.3).

While the objective in (9) enables degradation-agnostic training, it also introduces a mismatch between training and inference. During training, the denoiser is exposed only to clean speech corrupted by Gaussian noise, whereas at inference time X_t additionally contains environmental noise or interfering speakers inherited from the observation Y . We hypothesize that, despite this

mismatch, the denoiser learns to separate Gaussian perturbations from the underlying speech structure and thereby approximates the score function of clean speech. Consequently, it can still provide meaningful guidance toward regions of higher likelihood during inference, even in the presence of non-Gaussian or structured corruption. Our experimental results support this hypothesis and further suggest that a single prior model can generalize across different tasks, such as speech enhancement and speech separation.

4 Experimental Validation

4.1 Data representation

We follow [27] and operate in an amplitude-compressed short-time Fourier transform (STFT) domain using a hop length of 128, an FFT size and window length of 512, and a Hann window. The resulting complex-valued representation is converted into a two-channel real-valued tensor by stacking the real and imaginary components. Further details on the representation are provided in Appendix C.1.

4.2 Training data and implementation details

To train our denoiser models, we use clean speech from the 28-speaker training set of the VoiceBank-DEMAND dataset [38], with all audio signals downsampled to 16 kHz. We reserve the speakers p226 and p287 for the validation set. Our implementation is based on the EDM2SE repository [30], which employs the EDM2 [13] framework with a magnitude-preserved network architecture. Further implementation and training details are provided in Appendix C.2.

4.3 Evaluation metrics

We use objective instrumental metrics to evaluate the performance of our framework. SI-SDR [15] measures scale-invariant signal-to-distortion ratio in the time domain. PESQ [31] is an intrusive perceptual metric comparing enhanced speech to a clean reference. DNSMOS P.808 [26] as well as NISQA [25] and UTMOS [32] are non-intrusive, learning-based metrics that predict perceived speech quality without requiring a reference. We use QuartzNet15x5Base-En from the NVIDIA NeMo toolkit to compute the WER.

4.4 Speech enhancement

Test data. We consider two test conditions. In the matched condition, we use the VoiceBank-DEMAND [38] test set. In the mismatched condition, we evaluate on the EARS-WHAM (v2) test set [28], for which we additionally created manual text transcriptions available via the EARS-WHAM project page². All audio is resampled to 16 kHz. Compared to VoiceBank-DEMAND, EARS-WHAM contains a lower SNR range, making it a substantially more difficult test scenario.

Baselines. All baselines are trained on the same training data. We compare with SGMSE+ [27], a purely generative diffusion-based method. In addition, we include two hybrid methods, StoRM [17] and Diffiner [33]. We use the official implementations and the provided checkpoints. As predictors, we consider Conv-TasNet [22], NCSN++ [35] (predictor in StoRM [17]), and SEMamba [4]. We use the official implementations and the provided checkpoints except for Conv-TasNet, for which we use a third-party implementation³ and train the model with an SDR loss such that it is not scale-invariant.

Results. Figure 3 shows SI-SDR and NISQA performance as a function of the noise scaling parameter κ on the matched and mismatched validation sets. In the matched condition, both SI-SDR and NISQA perform best at lower values of κ . In the mismatched condition, increasing κ enables a trade-off between SI-SDR and NISQA, with NISQA improving as κ increases up to moderate values of κ . Based on these results, we use $\kappa = 0$ for the matched case and $\kappa = 0.4$ for the mismatched case in the following experiments. We use $M = 15$ sampling steps in all experiments. An ablation study on the number of sampling steps is provided in Appendix C.

²https://sp-uhh.github.io/ears_dataset/

³<https://github.com/kaituoxu/Conv-TasNet>

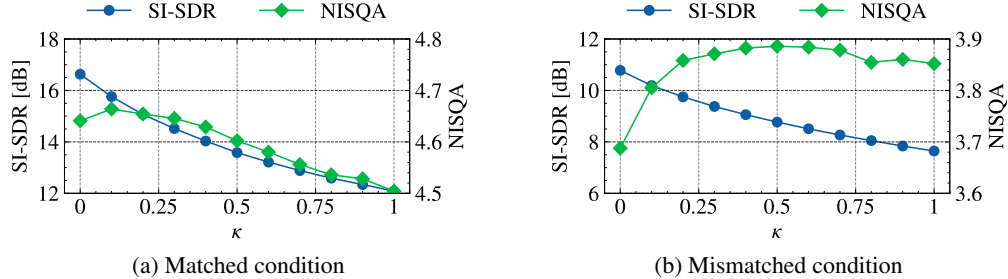


Figure 3: Speech enhancement performance over κ on the matched and mismatched validation sets.

Table 1: Speech enhancement results on the VoiceBank-DEMAND test set (mean scores). Best values are in bold, second-best are underlined. \dagger indicates that the score model was trained on outputs from NCSN++, thereby constituting a mismatch with the predictor used during inference.

	SI-SDR \uparrow [dB]	PESQ \uparrow	DNSMOS \uparrow [P.808]	NISQA \uparrow	UTMOS \uparrow	WER \downarrow [%]
Clean	inf	4.64	3.55	4.50	4.09	6.96
Noisy	8.44	1.97	3.09	3.03	3.11	11.01
SGMSE+ [27]	17.35	2.93	3.56	4.51	3.97	11.00
Diffiner [33]	17.55	2.67	3.49	4.79	3.99	14.65
Conv-TasNet [22]	18.57	2.51	3.31	3.45	3.61	11.87
+ StoRM \dagger [17]	11.99	2.31	3.36	3.93	3.65	16.87
+ StoRM [17]	17.92	2.67	3.54	4.57	3.92	13.32
+ Diffiner [33]	16.22	2.59	3.47	4.74	3.96	15.99
+ SIPS (ours)	18.79	2.64	3.43	4.28	3.85	12.86
NCSN++ [17]	19.57	2.83	3.59	4.64	3.93	9.58
+ StoRM [17]	18.49	2.89	3.56	4.52	3.92	10.21
+ Diffiner [33]	16.11	2.83	3.52	<u>4.80</u>	4.02	13.03
+ SIPS (ours)	19.20	2.88	3.56	4.72	3.97	10.00
SEMamba [4]	19.72	3.56	<u>3.58</u>	4.60	<u>4.07</u>	<u>8.87</u>
+ StoRM \dagger [17]	12.49	2.79	3.54	4.42	3.91	11.11
+ StoRM [17]	18.89	3.17	3.56	4.54	4.01	9.37
+ Diffiner [33]	16.51	2.87	3.53	4.81	4.04	12.43
+ SIPS (ours)	<u>19.63</u>	<u>3.43</u>	3.57	4.73	4.09	8.81

Table 1 reports the matched-condition results compared to the baselines. Across all predictors, SIPS slightly reduces the intrusive metrics (SI-SDR and PESQ) while consistently improving the non-intrusive perceptual metrics NISQA and UTMOS. Compared to existing hybrid approaches, however, the degradation in intrusive metrics is substantially smaller. For example, with SEMamba, SIPS preserves a high PESQ of 3.43 while still improving perceptual quality. Notably, SIPS also improves WER for SEMamba, whereas other hybrid methods degrade WER, potentially due to generative hallucinations introduced during sampling. StoRM performs worse when used with a mismatched predictor (indicated by \dagger). The publicly available pretrained StoRM model was trained with the NCSN++ predictor, and its performance degrades when evaluated with other predictors. Better results are obtained when the score model is trained on the output distribution of the corresponding predictor, indicating that StoRM is not naturally plug-and-play unlike SIPS and Diffiner. Although Diffiner achieves high NISQA scores, it substantially degrades the signal-level metrics, likely because posterior sampling introduces generative artifacts. In contrast, our plug-and-play framework yields only minor degradation in reference-based metrics while providing consistent improvements in perceptual quality. See Appendix C.7 for standard deviations on the metrics.

In the mismatched condition (Table 2), we observe similar trends but substantially higher WERs due to the more challenging SNR conditions and domain mismatch. SIPS consistently improves the non-intrusive quality metrics while maintaining comparable signal-level metrics. The elevated WERs

Table 2: Mismatched scenario: Speech enhancement results on the EARS-WHAM (v2) test set (mean scores). Best values are in bold, second-best are underlined. † indicates that the score model was trained on outputs from NCSN++, thereby constituting a mismatch with the predictor used during inference.

	SI-SDR ↑ [dB]	PESQ ↑	DNSMOS ↑ [P.808]	NISQA ↑	UTMOS ↑	WER ↓ [%]
Clean	inf	4.64	3.89	4.09	3.68	8.95
Noisy	5.36	1.24	2.73	1.95	1.68	32.87
SGMSE+ [27]	11.64	1.86	3.86	<u>4.09</u>	3.10	37.60
Conv-TasNet [22]	3.95	1.35	2.90	1.43	1.66	53.87
+ StoRM† [17]	-2.69	1.15	3.22	2.14	1.50	80.60
+ StoRM [17]	3.24	1.29	3.44	3.33	2.21	64.56
+ Diffiner [33]	-2.31	1.16	2.99	3.02	1.97	87.79
+ SIPS (ours)	3.86	1.32	3.09	1.98	1.73	59.10
NCSN++ [17]	13.24	1.81	3.72	3.84	2.75	<u>29.15</u>
+ StoRM [17]	<u>12.49</u>	1.90	<u>3.83</u>	4.12	2.86	31.74
+ Diffiner [33]	-0.11	1.30	<u>3.50</u>	3.40	2.22	69.05
+ SIPS (ours)	12.28	1.73	3.68	3.87	2.77	30.98
SEMamba [4]	11.36	2.19	3.71	3.57	2.93	28.08
+ StoRM† [17]	1.40	1.38	3.63	2.90	2.07	55.60
+ StoRM [17]	10.92	2.01	3.71	3.72	2.88	29.63
+ Diffiner [33]	4.88	1.43	3.44	3.67	2.53	64.21
+ SIPS (ours)	11.28	<u>2.05</u>	3.74	3.82	<u>2.97</u>	29.27

across hybrid approaches suggest generative hallucinations introduced during sampling. Although StoRM performs well under mismatch, it requires predictor-specific training and is therefore not plug-and-play. In contrast, Diffiner and SIPS are predictor-agnostic, though Diffiner struggles under mismatched conditions, particularly for Conv-TasNet and NCSN++. Interestingly, SGMSE+ achieves the highest DNSMOS and UTMOS scores, albeit at the cost of increased hallucinations reflected in the WER.

4.5 Speech separation

Test data. We use the monaural noisy reverberant subset of the WHAMR! dataset [23]. Its noisy speech mixtures are generated by convolving simulated room impulse responses with dry speech signals from the WSJ0-2mix [10] dataset and adding background noise.

Baselines. We consider two representative predictor models: a time-domain approach, SepFormer [37], and a time-frequency-domain one, FlexIO [24]. For SepFormer, we use the official checkpoint that was trained on the WHAMR! dataset⁴. Since the official model was trained with the SI-SDR loss [22], the scale of the separated signals can deviate from the true signals. This needs to be addressed in order to combine SepFormer with SIPS, which requires the predictor estimate to be at the correct scale. Difficulties in reproducing the public recipe prevented us from re-training the model with SNR loss, so we chose to use an oracle compensation of the scale ambiguity, matching each separated signal to the corresponding ground-truth after solving the speaker permutation based on SI-SDR. While this procedure is not applicable in practice, it provides insight into the achievable performance of the combination with SepFormer. There is no such issue with FlexIO, which is trained on a combination of multiple speech enhancement and separation datasets using the vanilla SNR loss [24]. We follow its large version, yielding the best performance on the WHAMR! dataset in the original paper. To measure WERs, we use QuartzNet15x5Base-En from the NVIDIA NeMo toolkit similarly to our enhancement experiments.

⁴<https://huggingface.co/speechbrain/sepformer-whamr16k>

Table 3: Speech separation results on WHAMR!. For the mixture, SI-SDR and PESQ are computed with respect to each speaker’s utterance and averaged.

Model	SI-SDR \uparrow [dB]	PESQ \uparrow	DNSMOS \uparrow [P.808]	NISQA \uparrow	UTMOS \uparrow	WER \downarrow [%]
Mixture	-7.20	1.08	2.53	1.21	1.35	92.62
SepFormer [37]	6.99	1.55	3.13	2.06	2.34	32.22
+ SIPS (ours)	6.79	1.41	3.36	3.01	2.60	34.29
FlexIO [24]	8.45	1.76	3.62	3.54	2.79	21.50
+ SIPS (ours)	8.51	1.56	3.68	4.01	3.01	23.43

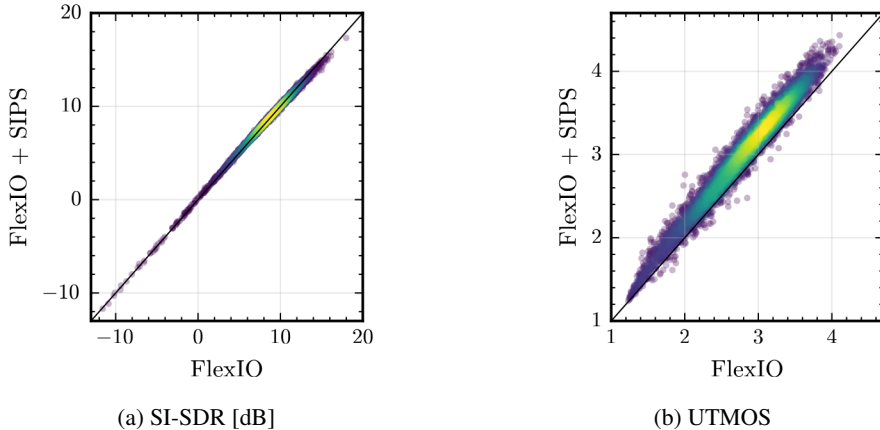


Figure 4: SI-SDR and UTMOS on WHAMR! for FlexIO with and without the generative prior. The diagonal line indicates equal performance. Individual test utterances are shown as points, with dense regions visualized as a density cloud.

Results. Table 3 summarizes separation performance on the WHAMR! dataset. For SIPS, we set the noise scale κ to 0. We observe a trend similar to speech enhancement, i.e., the combination with our prior improves non-intrusive metrics (DNSMOS, NISQA and UTMOS) with comparable SI-SDR. We also applied Diffiner to the outputs of both separation models. However, as reported in the follow-up work [11], Diffiner does not generalize well to speech separation, which we confirmed in our experiments. We therefore omit these results from Table 3. Unfortunately, the code for the method proposed in [11] is not publicly available, preventing a direct comparison.

Figure 4 presents the metrics distribution with and without our prior. The left panel demonstrates that our method with FlexIO does not change SI-SDR significantly, regardless of the performance of the initial separation. In contrast, the UTMOS score is consistently improved in the right panel.

5 Conclusion

In this work, we presented a plug-and-play framework for speech enhancement and separation that augments existing predictors with a generative speech prior. We refer to our method as SIPS (Stochastic Interpolant Prior for Speech), reflecting that the prior is applied incrementally in small sips. Built on stochastic interpolants, the method combines a predictor-induced drift with a score-based generative model trained only on clean speech, bridging predictive and generative modeling while remaining agnostic to the degradation process. Experiments with recent predictors, including SEMamba and FlexIO, demonstrate consistent improvements in perceptual speech quality, reflected by non-intrusive assessment metrics, while maintaining competitive performance on reference-based distortion measures and ASR-based WER evaluation. Overall, the results highlight the potential of combining strong predictors with generative priors to improve perceptual quality in speech restoration tasks such as speech enhancement and speech separation.

References

- [1] Michael S. Albergo and Eric Vanden-Eijnden. Building normalizing flows with stochastic interpolants. In *Proc. ICLR*, 2023.
- [2] Michael S. Albergo, Nicholas M. Boffi, and Eric Vanden-Eijnden. Stochastic interpolants: A unifying framework for flows and diffusions. *JMLR*, 26(209):1–80, 2025.
- [3] Shoko Araki, Nobutaka Ito, Reinhold Haeb-Umbach, Gordon Wichern, Zhong-Qiu Wang, and Yuki Mitsufuji. 30+ years of source separation research: Achievements and future challenges. In *Proc. IEEE ICASSP*, 2025.
- [4] Rong Chao, Wen-Huang Cheng, Moreno La Quatra, Sabato Marco Siniscalchi, Chao-Han Huck Yang, Szu-Wei Fu, and Yu Tsao. An investigation of incorporating Mamba for speech enhancement. In *Proc. IEEE SLT*, pages 302–308, 2024.
- [5] Ricky T. Q. Chen, Yulia Rubanova, Jesse Bettencourt, and David K Duvenaud. Neural ordinary differential equations. *Proc. NeurIPS*, 31, 2018.
- [6] Bhawana Chhaglani, Yang Gao, Julius Richter, Xilin Li, Syavosh Zadissa, Tarun Pruthi, and Andrew Lovitt. ArtiFree: Detecting and reducing generative artifacts in diffusion-based speech enhancement. In *Proc. IEEE ICASSP*, 2026.
- [7] Hyeong-Seok Choi, Jang-Hyun Kim, Jaesung Huh, Adrian Kim, Jung-Woo Ha, and Kyogu Lee. Phase-aware speech enhancement with deep complex U-Net. In *Proc. ICLR*, 2019. Retracted by the authors due to an experimental error (see OpenReview).
- [8] Valentin De Bortoli, James Thornton, Jeremy Heng, and Arnaud Doucet. Diffusion Schrödinger bridge with applications to score-based generative modeling. *Proc. NeurIPS*, 34:17695–17709, 2021.
- [9] Danilo de Oliveira, Julius Richter, Jean-Marie Lemerrier, Tal Peer, and Timo Gerkmann. On the behavior of intrusive and non-intrusive speech enhancement metrics in predictive and generative settings. In *Speech Communication; 15th ITG Conference*, pages 260–264. VDE, 2023.
- [10] John R. Hershey, Zhuo Chen, Jonathan Le Roux, and Shinji Watanabe. Deep clustering: Discriminative embeddings for segmentation and separation. In *Proc. IEEE ICASSP*, pages 31–35, 2016.
- [11] Masato Hirano, Ryosuke Sawata, Naoki Murata, Shusuke Takahashi, and Yuki Mitsufuji. Diffusion-based signal refiner for speech enhancement and separation. *IEEE Trans. Audio, Speech, Lang. Process.*, 2026.
- [12] Ante Jukić, Roman Korostik, Jagadeesh Balam, and Boris Ginsburg. Schrödinger bridge for generative speech enhancement. In *Proc. ISCA Interspeech*, pages 1175–1179, 2024.
- [13] Tero Karras, Miika Aittala, Jaakko Lehtinen, Janne Hellsten, Timo Aila, and Samuli Laine. Analyzing and improving the training dynamics of diffusion models. In *Proc. CVPR*, pages 24174–24184, 2024.
- [14] Bahjat Kawar, Michael Elad, Stefano Ermon, and Jiaming Song. Denoising diffusion restoration models. *Proc. NeurIPS*, 35:23593–23606, 2022.
- [15] Jonathan Le Roux, Scott Wisdom, Hakan Erdogan, and John R. Hershey. SDR–half-baked or well done? In *Proc. IEEE ICASSP*, pages 626–630, 2019.
- [16] Seonggyu Lee, Sein Cheong, Sangwook Han, and Jong Won Shin. FlowSE: Flow matching-based speech enhancement. In *Proc. IEEE ICASSP*, 2025.
- [17] Jean-Marie Lemerrier, Julius Richter, Simon Welker, and Timo Gerkmann. StoRM: A diffusion-based stochastic regeneration model for speech enhancement and dereverberation. *IEEE/ACM Trans. Audio, Speech, Lang. Process.*, 31:2724–2737, 2023.

- [18] Jean-Marie Lemerrier, Julius Richter, Simon Welker, Eloi Moliner, Vesa Välimäki, and Timo Gerkmann. Diffusion models for audio restoration: A review. *IEEE Signal Processing Magazine*, 41(6):72–84, 2025.
- [19] Kai Li, Guo Chen, Wendi Sang, Yi Luo, Zhuo Chen, Shuai Wang, Shulin He, Zhong-Qiu Wang, Andong Li, Zhiyong Wu, et al. Advances in speech separation: Techniques, challenges, and future trends. *arXiv preprint arXiv:2508.10830*, 2025.
- [20] Yaron Lipman, Ricky T. Q. Chen, Heli Ben-Hamu, Maximilian Nickel, and Matthew Le. Flow matching for generative modeling. In *Proc. ICLR*, 2023.
- [21] Xingchao Liu, Chengyue Gong, et al. Flow straight and fast: Learning to generate and transfer data with rectified flow. In *Proc. ICLR*, 2023.
- [22] Yi Luo and Nima Mesgarani. Conv-TasNet: Surpassing ideal time–frequency magnitude masking for speech separation. *IEEE/ACM Trans. Audio, Speech, Lang. Process.*, 27(8): 1256–1266, 2019.
- [23] Matthew Maciejewski, Gordon Wichern, Emmett McQuinn, and Jonathan Le Roux. WHAMR!: Noisy and reverberant single-channel speech separation. In *Proc. IEEE ICASSP*, pages 696–700, 2020.
- [24] Yoshiki Masuyama, Kohei Saijo, Francesco Paissan, Jiangyu Han, Marc Delcroix, Ryo Aihara, François G Germain, Gordon Wichern, and Jonathan Le Roux. FlexIO: Flexible single- and multi-channel speech separation and enhancement. In *Proc. IEEE ICASSP*, 2026.
- [25] Gabriel Mittag, Babak Naderi, Assmaa Chehadi, and Sebastian Möller. NISQA: A deep CNN-self-attention model for multidimensional speech quality prediction with crowdsourced datasets. In *Proc. ISCA Interspeech*, pages 2127–2131, 2021.
- [26] Chandan K. A. Reddy, Vishak Gopal, and Ross Cutler. DNSMOS: A non-intrusive perceptual objective speech quality metric to evaluate noise suppressors. In *Proc. IEEE ICASSP*, pages 6493–6497, 2021. doi: 10.1109/ICASSP39728.2021.9413882.
- [27] Julius Richter, Simon Welker, Jean-Marie Lemerrier, Bunlong Lay, and Timo Gerkmann. Speech enhancement and dereverberation with diffusion-based generative models. *IEEE/ACM Trans. Audio, Speech, Lang. Process.*, 31:2351–2364, 2023.
- [28] Julius Richter, Yi-Chiao Wu, Steven Krenn, Simon Welker, Bunlong Lay, Shinji Watanabe, Alexander Richard, and Timo Gerkmann. EARS: An anechoic fullband speech dataset benchmarked for speech enhancement and dereverberation. In *Proc. ISCA Interspeech*, pages 4873–4877, 2024.
- [29] Julius Richter, Danilo De Oliveira, and Timo Gerkmann. Investigating training objectives for generative speech enhancement. In *Proc. IEEE ICASSP*, 2025.
- [30] Julius Richter, Danilo de Oliveira, and Timo Gerkmann. Do we need EMA for diffusion-based speech enhancement? Toward a magnitude-preserving network architecture. In *Proc. IEEE ICASSP*, 2026.
- [31] Antony W Rix, John G Beerends, Michael P Hollier, and Andries P Hekstra. Perceptual evaluation of speech quality (PESQ)—a new method for speech quality assessment of telephone networks and codecs. In *Proc. IEEE ICASSP*, pages 749–752, 2001.
- [32] Takaaki Saeki, Detai Xin, Wataru Nakata, Tomoki Koriyama, Shinnosuke Takamichi, and Hiroshi Saruwatari. UTMOS: UTokyo-SaruLab system for VoiceMOS Challenge 2022. In *Proc. ISCA Interspeech*, pages 4521–4525, 2022.
- [33] Ryosuke Sawata, Naoki Murata, Yuhta Takida, Toshimitsu Uesaka, Takashi Shibuya, Shusuke Takahashi, and Yuki Mitsufuji. Diffiner: A versatile diffusion-based generative refiner for speech enhancement. In *Proc. ISCA Interspeech*, pages 3824–3828, 2023. doi: 10.21437/Interspeech.2023-1547.

- [34] Robin Scheibler, John R. Hershey, Arnaud Doucet, and Henry Li. Source separation by flow matching. In *Proc. IEEE WASPAA*, 2025.
- [35] Yang Song, Jascha Sohl-Dickstein, Diederik P Kingma, Abhishek Kumar, Stefano Ermon, and Ben Poole. Score-based generative modeling through stochastic differential equations. In *Proc. ICLR*, 2021.
- [36] Daniel Stoller, Sebastian Ewert, and Simon Dixon. Wave-U-Net: A multi-scale neural network for end-to-end audio source separation. In *Proc. ISMIR*, pages 334–340, 2018.
- [37] Cem Subakan, Mirco Ravanelli, Samuele Cornell, Mirko Bronzi, and Jianyuan Zhong. Attention is all you need in speech separation. In *Proc. IEEE ICASSP*, pages 21–25, 2021.
- [38] Cassia Valentini-Botinhao, Xin Wang, Shinji Takaki, and Junichi Yamagishi. Investigating RNN-based speech enhancement methods for noise-robust text-to-speech. In *Proc. ISCA SSW*, pages 146–152, 2016.
- [39] Simon Welker, Julius Richter, and Timo Gerkmann. Speech enhancement with score-based generative models in the complex STFT domain. In *Proc. ISCA Interspeech*, pages 2928–2932, 2022.
- [40] Simon Welker, Bunlong Lay, Maris Hillemann, Tal Peer, and Timo Gerkmann. Real-time streamable generative speech restoration with flow matching. *arXiv preprint arXiv:2512.19442*, 2025.

A Background on Stochastic Interpolants

Stochastic interpolants [1, 2] provide a continuous-time formulation for constructing transport maps between probability distributions. They offer a unified view of flow-based models [20, 21], score-based diffusion bridge models [35], and related transport-based generative modeling methods such as the Schrödinger bridge [8]. In this appendix, we briefly summarize the main concepts used in Section 3.

A.1 Dynamical transport of probability measures

Let ρ_0 and ρ_1 denote two probability densities on \mathbb{R}^d . Generative modeling can be viewed as the problem of constructing a transport from a base distribution ρ_0 to a target distribution ρ_1 . A deterministic flow map $X_t : \mathbb{R}^d \rightarrow \mathbb{R}^d$ is induced by a velocity field $b(t, x)$ through the ODE [5]

$$\frac{d}{dt}X_t(x) = b(t, X_t(x)), \quad X_0(x) = x. \quad (10)$$

If X_t has density $\rho(t, \cdot)$, then ρ evolves according to the transport equation

$$\partial_t \rho(t, x) + \nabla \cdot (b(t, x)\rho(t, x)) = 0. \quad (11)$$

Thus, if $\rho(0, \cdot) = \rho_0$ and $\rho(1, \cdot) = \rho_1$, the flow defines a continuous transport from ρ_0 to ρ_1 .

A.2 Definition of stochastic interpolants

Given two endpoint variables $X_0 \sim \rho_0$ and $X_1 \sim \rho_1$, a stochastic interpolant is a family of random variables

$$X_t = f(t, X_0, X_1) + \gamma(t)Z, \quad t \in [0, 1], \quad (12)$$

where $Z \sim \mathcal{N}(0, I)$ is independent of (X_0, X_1) , $f : [0, 1] \times \mathbb{R}^d \times \mathbb{R}^d \rightarrow \mathbb{R}^d$ is a sufficiently smooth interpolation function, and $\gamma : [0, 1] \rightarrow \mathbb{R}_{\geq 0}$ is a scalar noise schedule. The interpolation function satisfies the endpoint conditions

$$f(0, X_0, X_1) = X_0, \quad f(1, X_0, X_1) = X_1, \quad (13)$$

and the noise schedule satisfies

$$\gamma(0) = \gamma(1) = 0, \quad \gamma(t) > 0 \quad \text{for } t \in (0, 1). \quad (14)$$

Consequently, X_t has endpoint distributions ρ_0 and ρ_1 by construction.

A common example is the linear stochastic interpolant

$$X_t = (1 - t)X_0 + tX_1 + \gamma(t)Z. \quad (15)$$

In this paper, we use this form with $X_0 = Y$ denoting corrupted speech and $X_1 = S$ denoting clean speech. Writing the observation as $Y = S + N$, where N denotes environmental noise, the interpolant can be rewritten as

$$X_t = S + (1 - t)N + \gamma(t)Z, \quad (16)$$

which provides the interpretation of gradually removing the environmental noise component or the interfering speaker while injecting controlled stochasticity.

A.3 Velocity field and drift decomposition

The time derivative of the interpolant is

$$\dot{X}_t = \partial_t f(t, X_0, X_1) + \dot{\gamma}(t)Z. \quad (17)$$

The velocity field $b(t, x)$ in (11) is defined as the conditional expectation

$$b(t, x) = \mathbb{E}[\dot{X}_t | X_t = x]. \quad (18)$$

See Appendix B.1 for a proof. Thus, the stochastic interpolant induces a deterministic probability flow that transports the endpoint density ρ_0 to ρ_1 .

For the linear interpolant

$$X_t = (1-t)X_0 + tX_1 + \gamma(t)Z, \quad (19)$$

we obtain

$$\dot{X}_t = X_1 - X_0 + \dot{\gamma}(t)Z, \quad (20)$$

and therefore

$$b(t, x) = \mathbb{E}[X_1 - X_0 + \dot{\gamma}(t)Z | X_t = x]. \quad (21)$$

In this work, we exploit the fact that this velocity can be written as

$$b(t, x) = v(t, x) + \dot{\gamma}(t)\eta_z(t, x), \quad (22)$$

where

$$v(t, x) = \mathbb{E}[X_1 - X_0 | X_t = x], \quad \eta_z(t, x) = \mathbb{E}[Z | X_t = x]. \quad (23)$$

A.4 Regression objectives

The velocity field v can be learned by minimizing the quadratic objective

$$\mathcal{L}_b(\hat{v}) := \int_0^1 \mathbb{E}_{X_0, X_1, Z} \left[\|\hat{v}(t, X_t) - \partial_t f(t, X_0, X_1)\|^2 \right] dt, \quad (24)$$

where the expectation is taken over the random variables defining the interpolant process X_t . The unique minimizer of (24) is given by the conditional expectation in Theorem 7 of [2]. Similarly, the denoising term $\eta_z(t, x) = \mathbb{E}[Z | X_t = x]$ can be learned via

$$\mathcal{L}_\eta(\hat{\eta}) := \int_0^1 \mathbb{E}_{X_0, X_1, Z} \left[\|\hat{\eta}(t, X_t) - Z\|^2 \right] dt, \quad (25)$$

whose unique minimizer is likewise given by the corresponding conditional expectation [2, Theorem 7].

A.5 ODE and SDE samplers

The transport equation above induces the deterministic probability flow ODE

$$\frac{d}{dt} X_t = b(t, X_t), \quad (26)$$

as defined in (10). The same time marginals $\rho(t, \cdot)$ can also be realized by a family of stochastic differential equations. In particular, adding a diffusion term with variance schedule $\epsilon(t) \geq 0$ requires a corresponding correction of the drift to preserve the same marginals, as shown by the Fokker–Planck equation (see Appendix B.2). For any diffusion schedule $\epsilon(t) \geq 0$, define

$$b_F(t, x) = b(t, x) + \epsilon(t)\nabla_x \log \rho(t, x). \quad (27)$$

Then the forward SDE

$$dX_t^F = b_F(t, X_t^F) dt + \sqrt{2\epsilon(t)} dW_t \quad (28)$$

has the same marginal density $\rho(t, \cdot)$ as the interpolant. Using the denoiser-score relation

$$\nabla_x \log \rho(t, x) = -\gamma(t)^{-1}\eta_z(t, x), \quad (29)$$

the forward drift can be written as

$$b_F(t, x) = b(t, x) - \epsilon(t)\gamma(t)^{-1}\eta_z(t, x). \quad (30)$$

For the decomposition

$$b(t, x) = v(t, x) + \dot{\gamma}(t)\eta_z(t, x), \quad (31)$$

the forward drift becomes

$$b_F(t, x) = v(t, x) + \left(\dot{\gamma}(t) - \frac{\epsilon(t)}{\gamma(t)} \right) \eta_z(t, x). \quad (32)$$

The sampler used in the main text corresponds to the choice

$$\epsilon(t) = \kappa\gamma(t), \quad (33)$$

which yields

$$dX_t^F = [v(t, X_t^F) + (\dot{\gamma}(t) - \kappa)\eta_z(t, X_t^F)] dt + \sqrt{2\kappa\gamma(t)} dW_t. \quad (34)$$

This is the SDE formulation used in Section 3. When $\kappa = 0$, the stochastic term vanishes and the sampler reduces to the corresponding probability flow ODE.

B Proofs

B.1 Proof that the interpolant density satisfies the transport equation

We follow the derivations in Appendix B of Albergo et al. [2]. Let

$$X_t = f(t, X_0, X_1) + \gamma(t)Z, \quad (35)$$

with time derivative

$$\dot{X}_t = \partial_t f(t, X_0, X_1) + \dot{\gamma}(t)Z. \quad (36)$$

We define the velocity field

$$b(t, x) := \mathbb{E}[\dot{X}_t | X_t = x]. \quad (37)$$

Let $\rho(t, x)$ denote the density of X_t . We show that ρ satisfies

$$\partial_t \rho(t, x) + \nabla_x \cdot (b(t, x)\rho(t, x)) = 0. \quad (38)$$

Consider the characteristic function of X_t ,

$$\varphi_{X_t}(t, k) := \mathbb{E} [e^{ik \cdot X_t}] = \int_{\mathbb{R}^d} e^{ik \cdot x} \rho(t, x) dx. \quad (39)$$

Differentiating with respect to time gives

$$\partial_t \varphi_{X_t}(t, k) = \mathbb{E} [ik \cdot \dot{X}_t e^{ik \cdot X_t}] = ik \cdot m(t, k), \quad (40)$$

where

$$m(t, k) := \mathbb{E} [\dot{X}_t e^{ik \cdot X_t}]. \quad (41)$$

Using the law of total expectation, we can write

$$\begin{aligned} m(t, k) &= \mathbb{E} [\mathbb{E}[\dot{X}_t e^{ik \cdot X_t} | X_t]] \\ &= \mathbb{E} [e^{ik \cdot X_t} \mathbb{E}[\dot{X}_t | X_t]] \\ &= \int_{\mathbb{R}^d} e^{ik \cdot x} b(t, x) \rho(t, x) dx. \end{aligned} \quad (42)$$

Therefore,

$$\partial_t \varphi_{X_t}(t, k) = ik \cdot \int_{\mathbb{R}^d} e^{ik \cdot x} b(t, x) \rho(t, x) dx. \quad (43)$$

On the other hand, differentiating the density representation gives

$$\partial_t \varphi_{X_t}(t, k) = \int_{\mathbb{R}^d} e^{ik \cdot x} \partial_t \rho(t, x) dx. \quad (44)$$

Thus, for all $k \in \mathbb{R}^d$,

$$\int_{\mathbb{R}^d} e^{ik \cdot x} \partial_t \rho(t, x) dx = ik \cdot \int_{\mathbb{R}^d} e^{ik \cdot x} b(t, x) \rho(t, x) dx. \quad (45)$$

Since

$$\int_{\mathbb{R}^d} e^{ik \cdot x} \nabla \cdot (b(t, x)\rho(t, x)) dx = -ik \cdot \int_{\mathbb{R}^d} e^{ik \cdot x} b(t, x) \rho(t, x) dx, \quad (46)$$

where we used the Fourier transform identity $\mathcal{F}[\nabla \cdot g](k) = -ik \cdot \mathcal{F}[g](k)$, we obtain

$$\int_{\mathbb{R}^d} e^{ik \cdot x} [\partial_t \rho(t, x) + \nabla \cdot (b(t, x)\rho(t, x))] dx = 0. \quad (47)$$

The left-hand side is the Fourier transform of $\partial_t \rho(t, x) + \nabla \cdot (b(t, x)\rho(t, x))$. Since this transform vanishes for all $k \in \mathbb{R}^d$, and the Fourier transform is injective on integrable functions, the integrand itself must vanish almost everywhere. Hence,

$$\partial_t \rho(t, x) + \nabla \cdot (b(t, x)\rho(t, x)) = 0. \quad (48)$$

This proves that the interpolant density satisfies the transport equation.

B.2 Proof of the equivalent SDE marginals

We show that the forward SDE in (28) has the same time marginals as the interpolant. The interpolant density $\rho(t, x)$ satisfies the transport equation

$$\partial_t \rho(t, x) + \nabla_x \cdot (b(t, x)\rho(t, x)) = 0. \quad (49)$$

The Fokker–Planck equation associated with the forward SDE is

$$\partial_t \rho(t, x) = -\nabla_x \cdot (b_F(t, x)\rho(t, x)) + \epsilon(t)\Delta_x \rho(t, x). \quad (50)$$

Substituting

$$b_F(t, x) = b(t, x) + \epsilon(t)\nabla_x \log \rho(t, x) \quad (51)$$

gives

$$\partial_t \rho(t, x) = -\nabla_x \cdot (b(t, x)\rho(t, x)) - \epsilon(t)\nabla_x \cdot (\rho(t, x)\nabla_x \log \rho(t, x)) + \epsilon(t)\Delta_x \rho(t, x) \quad (52)$$

$$= -\nabla_x \cdot (b(t, x)\rho(t, x)) - \epsilon(t)\Delta_x \rho(t, x) + \epsilon(t)\Delta_x \rho(t, x) \quad (53)$$

$$= -\nabla_x \cdot (b(t, x)\rho(t, x)). \quad (54)$$

Thus, the Fokker–Planck equation reduces to the original transport equation. Consequently, the forward SDE and the probability flow ODE share the same time marginals $\rho(t, \cdot)$.

C Implementation Details and Ablations

C.1 Data representation

Following [27], we operate in an amplitude-compressed time–frequency domain using the STFT with a hop length of 128, an FFT size and window length of 512, using a Hann window. Let F denote the number of frequency bins and K the number of time frames. For each coefficient $\tilde{x}_{fk} \in \mathbb{C}$ of the STFT, where $f \in \{1, \dots, F\}$ and $k \in \{1, \dots, K\}$, we define the representation as

$$x_{fk} = b |\tilde{x}_{fk}|^p e^{i\angle \tilde{x}_{fk}}, \quad (55)$$

where $p \in (0, 1]$ denotes a compression exponent (set to $p = 0.5$ in our experiments), $b \in \mathbb{R}_+$ is a scaling factor used to normalize amplitudes (set to $b = 0.15$), and $\angle(\cdot)$ denotes the phase of a complex number. The real and imaginary components are separated and stacked along a channel dimension, resulting in a tensor representation in $\mathbb{R}^{C \times F \times K}$ with $C = 2$. This representation naturally supports processing with two-dimensional convolutional architectures over time and frequency.

C.2 Implementation and Training Details

Our implementation is based on the repository⁵ of EDM2SE [30], which employs the EDM2 [13] framework with a magnitude-preserved network architecture. All denoiser models are trained on two NVIDIA A40 GPUs with a total batch size of 16 (2×8) for approximately 4.2M training samples of about 2 s of clean speech, taking roughly two to three days. We employ an inverse square root learning rate decay schedule with an initial learning rate of 2.5×10^{-3} . The learning rate linearly ramps up during the first 1M training samples, while inverse square root decay is applied starting from 0.48M samples.

C.3 Hyperparameter Selection for the Noise Schedule

We study the influence of the hyperparameters a and c , which control the stochastic interpolation noise schedule, on the speech enhancement performance. The noise scale $\gamma(t)$ and its derivative $\dot{\gamma}(t)$ are visualized in Figure 5 for $t \in [0, 1]$, where c controls the amplitude of the schedule, while a introduces an offset to $\gamma(t)$. To determine suitable values, we perform a grid search on VoiceBank-DEMAND while keeping all other training and inference settings fixed. The evaluated configurations are summarized in Table 4.

The results show that the choice of noise schedule parameters has a noticeable impact on both perceptual quality and distortion-based metrics. We observe that setting $a = 0.0$ leads to unstable

⁵<https://github.com/sp-uhh/edm2se>

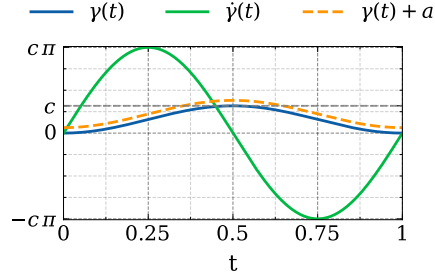


Figure 5: Visualization of the interpolation noise schedule $\gamma(t)$ and its derivative $\dot{\gamma}(t)$ for $t \in [0, 1]$. The parameter c controls the amplitude of the schedule, while a adds an offset to $\gamma(t)$.

Table 4: Speech enhancement results on VoiceBank-DEMAND for different noise schedule hyperparameters a and c .

	a	c	SI-SDR \uparrow [dB]	PESQ \uparrow	NISQA \uparrow	UTMOS \uparrow
Noisy	-	-	8.44	1.97	3.03	3.11
SEMamba	-	-	19.72	3.56	4.60	4.07
+ SIPS	0.0	0.3	-71.22	1.10	1.55	3.28
+ SIPS	0.0	0.5	-71.22	1.10	1.55	3.28
+ SIPS	0.001	0.1	19.10	3.45	4.63	4.11
+ SIPS	0.001	0.5	19.22	3.18	4.74	4.11
+ SIPS	0.01	2.0	17.61	2.89	4.76	4.07
+ SIPS	0.05	0.0	19.08	3.53	4.65	4.11
+ SIPS	0.05	0.5	19.23	3.37	4.75	4.11
+ SIPS	0.05	1.0	18.74	3.27	4.77	4.11
+ SIPS	0.05	2.0	17.39	3.13	4.80	4.10
+ SIPS	0.05	3.0	16.32	2.91	4.80	4.07
+ SIPS	0.05	4.0	14.66	2.69	4.77	4.00
+ SIPS	0.1	0.0	19.08	3.53	4.65	4.11
+ SIPS	0.1	0.1	19.20	3.51	4.68	4.11
+ SIPS	0.1	0.3	19.28	3.44	4.71	4.10
+ SIPS	0.1	0.5	19.15	3.40	4.74	4.10
+ SIPS	0.1	1.0	19.06	3.32	4.78	4.08
+ SIPS	0.1	2.0	16.92	3.11	4.79	4.08
+ SIPS	0.2	0.0	19.08	3.53	4.65	4.11
+ SIPS	0.2	0.1	19.27	3.50	4.66	4.09
+ SIPS	0.2	0.3	19.17	3.40	4.65	4.08

training and consistently poor performance across metrics. In contrast, overly large values of c tend to degrade SI-SDR, indicating reduced reconstruction fidelity. Based on the overall trade-off between distortion-based and perceptual metrics, we select $a = 0.1$ and $c = 0.5$ for all subsequent experiments, as this configuration provides the most balanced performance across evaluation criteria.

C.4 Effect of the Number of Sampling Steps

We analyze the impact of the number of sampling steps N using the validation sets. Figure 6a presents the speech enhancement performance under matched conditions, while Figure 6b reports the corresponding results for mismatched noise conditions. Overall, performance improves with increasing N before saturating, indicating a trade-off between inference cost and enhancement quality. Based on these results, we use $N = 15$ sampling steps as the default setting in all subsequent experiments.

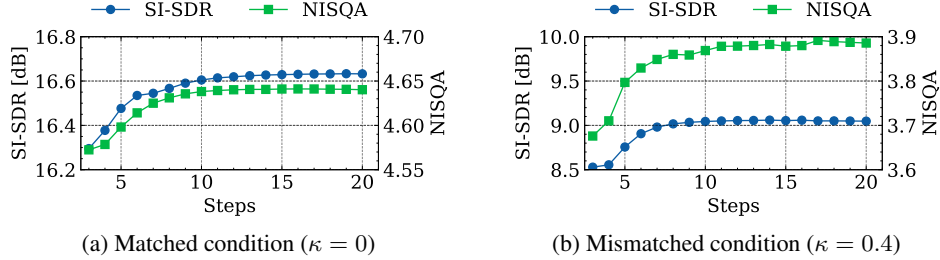


Figure 6: Speech enhancement performance over number of steps N on the matched and mismatched validation sets.

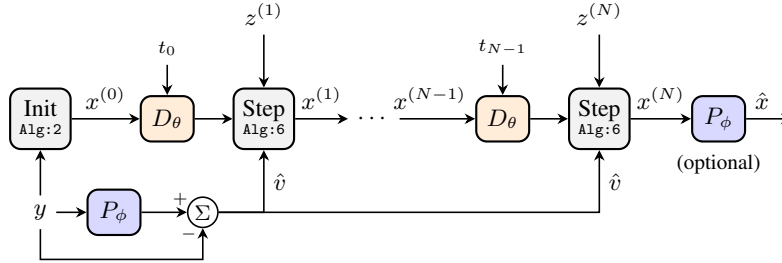


Figure 7: Schematic of the proposed framework. The predictor P_ϕ defines a deterministic drift $\hat{v} = P_\phi(y) - y$ from the observation y , which steers the sampling dynamics at every step. Concurrently, the denoiser D_θ guides the trajectory toward regions of higher likelihood. After the sampling procedure, the predictor is optionally applied again as a post-processing step.

C.5 Effect of the Postprocessing After Generative Sampling

Figure 7 illustrates the processing pipeline, including the optional post-processing step in which the predictor is applied again after sampling. Tables 5 and 6 report the results with and without post-processing for the matched and mismatched conditions, respectively. Overall, post-processing does not provide consistent improvements across the evaluation metrics, and in some cases slightly degrades performance. Therefore, we do not employ post-processing in the main experiments presented in the paper.

C.6 Diffiner with reduced sampling steps

To compare computational efficiency under a similar sampling budget, we additionally evaluate Diffiner using only $M = 15$ sampling steps. The corresponding results on the VoiceBank-DEMAND

Table 5: Speech enhancement results on the VoiceBank-DEMAND test set (mean scores)

	SI-SDR \uparrow [dB]	PESQ \uparrow	DNSMOS \uparrow [P.808]	NISQA \uparrow	UTMOS \uparrow	WER \downarrow [%]
Noisy	8.44	1.97	3.09	3.03	3.11	11.01
Conv-TasNet [22]	18.57	2.51	3.31	3.45	3.61	11.87
+ SIPS (w post)	18.34	2.52	3.41	4.04	3.84	12.91
+ SIPS (w/o post)	18.79	2.64	3.43	4.28	3.85	12.86
NCSN++ [17]	19.57	2.83	3.59	4.64	3.93	9.58
+ SIPS (w post)	18.53	2.70	3.57	4.70	3.97	9.97
+ SIPS (w/o post)	19.20	2.88	3.56	4.72	3.97	10.00
SEMamba [4]	19.72	3.56	3.58	4.60	4.07	8.87
+ SIPS (w post)	19.16	3.41	3.58	4.76	4.12	8.71
+ SIPS (w/o post)	19.63	3.43	3.57	4.73	4.09	8.81

Table 6: Mismatched scenario: Speech enhancement results on the EARS-WHAM (v2) test set.

	SI-SDR \uparrow [dB]	PESQ \uparrow	DNSMOS \uparrow [P.808]	NISQA \uparrow	UTMOS \uparrow	WER \downarrow [%]
Noisy	5.36	1.24	2.73	1.95	1.68	32.87
Conv-TasNet [22]	3.95	1.35	2.90	1.43	1.66	53.87
+ SIPS (w post)	3.28	1.33	3.20	2.37	1.85	67.07
+ SIPS (w/o post)	3.86	1.32	3.09	1.98	1.73	59.10
NCSN++ [17]	13.24	1.81	3.72	3.84	2.75	29.15
+ SIPS (w post)	10.62	1.66	3.72	4.09	2.79	35.56
+ SIPS (w/o post)	12.28	1.73	3.68	3.87	2.77	30.98
SEMamba [4]	11.36	2.19	3.71	3.57	2.93	28.08
+ SIPS (w post)	9.69	1.97	3.75	3.86	2.95	36.26
+ SIPS (w/o post)	11.28	2.05	3.74	3.82	2.97	29.27

Table 7: Speech enhancement results on the VoiceBank-DEMAND test set.

	SI-SDR \uparrow [dB]	PESQ \uparrow	DNSMOS \uparrow [P.808]	NISQA \uparrow	UTMOS \uparrow	WER \downarrow [%]
Noisy	8.44	1.97	3.09	3.03	3.11	11.01
Conv-TasNet [22]	18.57	2.51	3.31	3.45	3.61	11.87
+ Diffiner [33] (M=200)	16.22	2.59	3.47	4.74	3.96	15.99
+ Diffiner [33] (M=15)	13.05	2.07	3.22	4.43	3.64	31.41
+ SIPS (M=15)	18.79	2.64	3.43	4.28	3.85	12.86
NCSN++ [17]	19.57	2.83	3.59	4.64	3.93	9.58
+ Diffiner [33] (M=200)	16.11	2.83	3.52	4.80	4.02	13.03
+ Diffiner [33] (M=15)	13.05	2.16	3.26	4.52	3.69	29.59
+ SIPS (M=15)	19.20	2.88	3.56	4.72	3.97	10.00
SEMamba [4]	19.72	3.56	3.58	4.60	4.07	8.87
+ Diffiner [33] (M=200)	16.51	2.87	3.53	4.81	4.04	12.43
+ Diffiner [33] (M=15)	13.18	2.19	3.29	4.56	3.72	26.23
+ SIPS (M=15)	19.63	3.43	3.57	4.73	4.09	8.81

dataset are reported in Table 7. Compared to the default configuration with 200 sampling steps, Diffiner exhibits a significant performance drop when the number of steps is reduced to 15. In contrast, SIPS maintains strong performance with $M = 15$ sampling steps, highlighting the computational efficiency of our approach.

C.7 Results with standard deviations

In addition to the averaged metrics reported in the main paper, we provide the corresponding standard deviations for the main experimental results in the following tables.

Table 8: Speech enhancement results on the VoiceBank-DEMAND test set (mean \pm standard deviation). Best values are in bold and second-best are underlined.

	SI-SDR \uparrow [dB]	PESQ \uparrow	NISQA \uparrow	UTMOS \uparrow
Clean	-	4.64 ± 0.00	4.50 ± 0.30	4.09 ± 0.19
Noisy	8.44 ± 5.61	1.97 ± 0.75	3.03 ± 0.82	3.11 ± 0.76
SGMSE+ [27]	17.35 ± 3.33	2.93 ± 0.62	4.51 ± 0.38	3.97 ± 0.24
Diffiner [33]	17.55 ± 3.70	2.67 ± 0.70	4.79 ± 0.32	3.99 ± 0.26
Conv-TasNet [22]	18.57 ± 3.57	2.51 ± 0.63	3.45 ± 0.72	3.61 ± 0.47
+ StoRM [†] [17]	11.99 ± 1.72	2.31 ± 0.58	3.93 ± 0.58	3.65 ± 0.43
+ StoRM [17]	17.92 ± 3.30	2.67 ± 0.65	4.57 ± 0.34	3.92 ± 0.29
+ Diffiner [33]	16.22 ± 3.68	2.59 ± 0.69	4.74 ± 0.27	3.96 ± 0.27
+ SIPS (ours)	18.79 ± 3.57	2.64 ± 0.73	4.28 ± 0.51	3.85 ± 0.39
NCSN++ [17]	19.57 ± 3.59	2.83 ± 0.72	4.64 ± 0.42	3.93 ± 0.31
+ StoRM [17]	18.49 ± 3.40	2.89 ± 0.65	4.52 ± 0.36	3.92 ± 0.28
+ Diffiner [33]	16.11 ± 3.26	2.83 ± 0.73	<u>4.80 ± 0.25</u>	4.02 ± 0.25
+ SIPS (ours)	19.20 ± 3.26	2.88 ± 0.82	4.72 ± 0.34	3.97 ± 0.31
SEMamba [4]	19.72 ± 3.22	3.56 ± 0.60	4.60 ± 0.37	4.07 ± 0.24
+ StoRM [†] [17]	12.49 ± 1.55	2.79 ± 0.57	4.42 ± 0.42	3.91 ± 0.29
+ StoRM [17]	18.89 ± 3.06	3.17 ± 0.58	4.54 ± 0.30	4.01 ± 0.25
+ Diffiner [33]	16.51 ± 3.29	2.87 ± 0.73	4.81 ± 0.25	4.04 ± 0.24
+ SIPS (ours)	<u>19.63 ± 3.14</u>	<u>3.43 ± 0.69</u>	4.73 ± 0.30	4.09 ± 0.24